Electronic Supplementary Material (ESI) for Dalton Transactions.

Supplementary Information

Alkyl-dependent self-assembly of the first red-emitting zwitterionic {Cu_4I_6} clusters from [Alkyl–P(2-Py)$_3$]$^+$ salts and CuI: when size matters

Alexander V. Artem'ev,*[a,b] Elena A. Pritchina,[b,c] Mariana I. Rakhmanova,[a,b] Nina P. Gritsan,*[b,c] Irina Yu. Bagryanskaya,[b,d] Svetlana F. Malysheva[e] and Nataliya A. Belogorlova[e]

[a] *Nikolaev Institute of Inorganic Chemistry, Siberian Branch of Russian Academy of Sciences, 3, Akad. Lavrentiev Ave., Novosibirsk 630090, Russian Federation*
[b] *Novosibirsk State University, (National Research University), Department of Natural Sciences, 2, Pirogova Str., Novosibirsk 630090, Russian Federation*
[c] *Voevodsky Institute of Chemical Kinetics and Combustion, Institutskaya str. 3, 630090 Novosibirsk, Russian Federation*
[d] *N. N. Vorozhtsov Novosibirsk Institute of Organic Chemistry, Siberian Branch of Russian Academy of Sciences, 9, Akad. Lavrentiev Ave., Novosibirsk 630090, Russian Federation*
[e] *A. E. Favorsky Irkutsk Institute of Chemistry, Siberian Branch of the Russian Academy of Sciences, 1 Favorsky Str., 664033 Irkutsk, Russian Federation*

*Corresponding authors: chemisufarm@yandex.ru (Alexander V. Artem'ev), gritsan@kinetics.nsc.ru (Nina P. Gritsan).

Table of Contents

Pages

S2–6 §1. X-Ray crystallography
S6–7 §2. Thermogravimetry
S7–9 §3. FT-IR spectra
S10–13 §4. ^{1}H and ^{31}P{^{1}H} NMR spectra
S13–14 §5. ESI-MS spectra
S15–16 §6. Photophysical data
S16–21 §7. Computational details
S22 §8. References

§1. X-Ray crystallography

Table S1. Data collection and selected refinement parameters for complexes **1**–**4**.

Compound	**1**·2MeCN	**2** (at 200 K)	**2** (at 296 K)	**3**	**4**
CCDC number	1579827	1579828		1579829	1579830
Empirical formula	$C_{36}H_{36}Cu_4I_6N_8P_2$	$C_{36}H_{38}Cu_4I_6N_6P_2$	$C_{36}H_{38}Cu_4I_6N_6P_2$	$C_{38}H_{42}Cu_4I_6N_6P_2$	$C_{44}H_{38}Cu_4I_6N_6P_2$
Formula mass [g/mol]	1658.23	1632.22	1632.22	1660.27	1728.30
Space group	$P2_1/c$	*C*2/*c*	*C*2/*c*	*P*–1	*P*–1
a [Å]	9.4058(3)	23.5747(6)	23.6729(10)	10.2369(13)	10.1053(4)
b [Å]	14.5684(5)	12.1144(4)	12.2107(5)	11.9900(14)	12.2864(5)
c [Å]	35.3521(11)	17.7008(5)	17.7600(6)	12.2061(15)	12.3397(6)
α [°]	90.00	90.00	90.00	118.729(5)	118.947(2)
β [°]	94.4820(10)	114.1870(10)	114.074(1)	93.281(6)	92.187(2)
γ [°]	90.00	90.00	90.00	107.283(6)	107.225(2)
V [$Å^3$]	4829.4(3)	3354.6(3)	4687.2(3)	1218.1(3)	1249.98(10)
Z	4	4	4	1	1
Crystal size [mm]	0.800 × 0.100 × 0.040	0.400 × 0.300 × 0.300	0.40 × 0.30 × 0.15	0.350 × 0.250 × 0.150	0.400 × 0.400 × 0.200
$D_{calcd.}$ [g·cm^{-3}]	2.281	2.351	2.313	2.263	2.296
μ [mm^{-1}]	5.675	5.940	5.844	5.623	5.485
Temperature [K]	200(2)	200(2)	296(2)	299(2)	296(2)
Reflections collected	88780	43842	27512	33936	35481
Independent reflections	14136 [R_{int} = 0.0426]	6339 [R_{int} = 0.0298]	5359 [R_{int} = 0.0493]	5576 [R_{int} = 0.0707]	5118 [R_{int} = 0.0334]
Reflections with $I > 2\sigma(I)$	11647	5841	4594	4607	4772
R_1, wR_2 [$I > 2\sigma(I)$]	0.0296, 0.0787	0.0199, 0.0437	0.0259, 0.0569	0.0639, 0.1602	0.0293, 0.0802
R_1, wR_2 (all data)	0.0416, 0.0858	0.0230, 0.0447	0.0339, 0.0605	0.0760, 0.1792	0.0318, 0.0829
Goodness of fit	1.043	1.081	1.033	1.043	1.022
Largest diff peak and hole [e/$Å^3$]	1.20 and –1.32	1.56 and –1.44	1.60 and –1.31	2.57 and –2.36	2.37 and –1.40

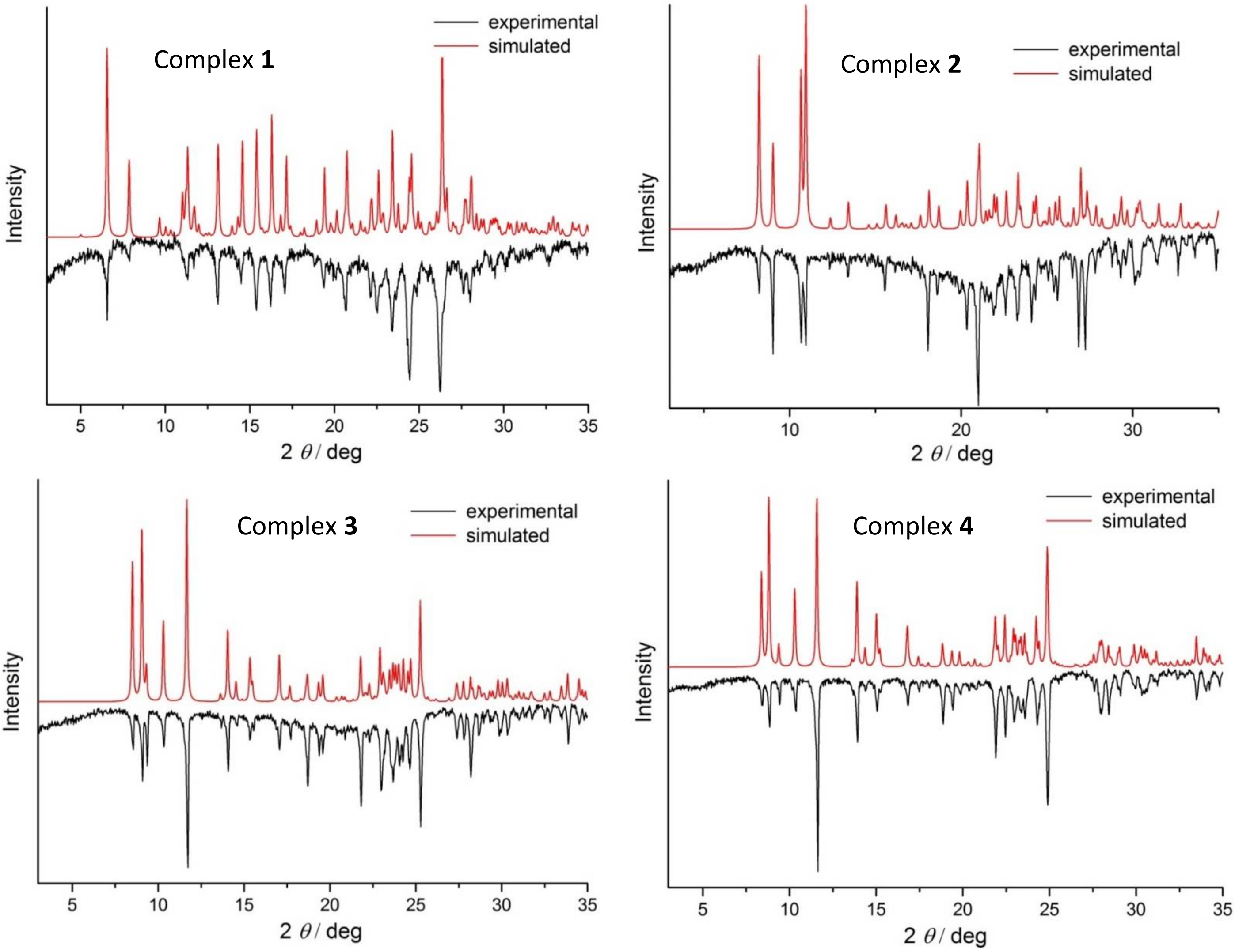

Figure S1. Experimental and simulated XRPD patterns of as-synthesized samples of **1**–**4**.

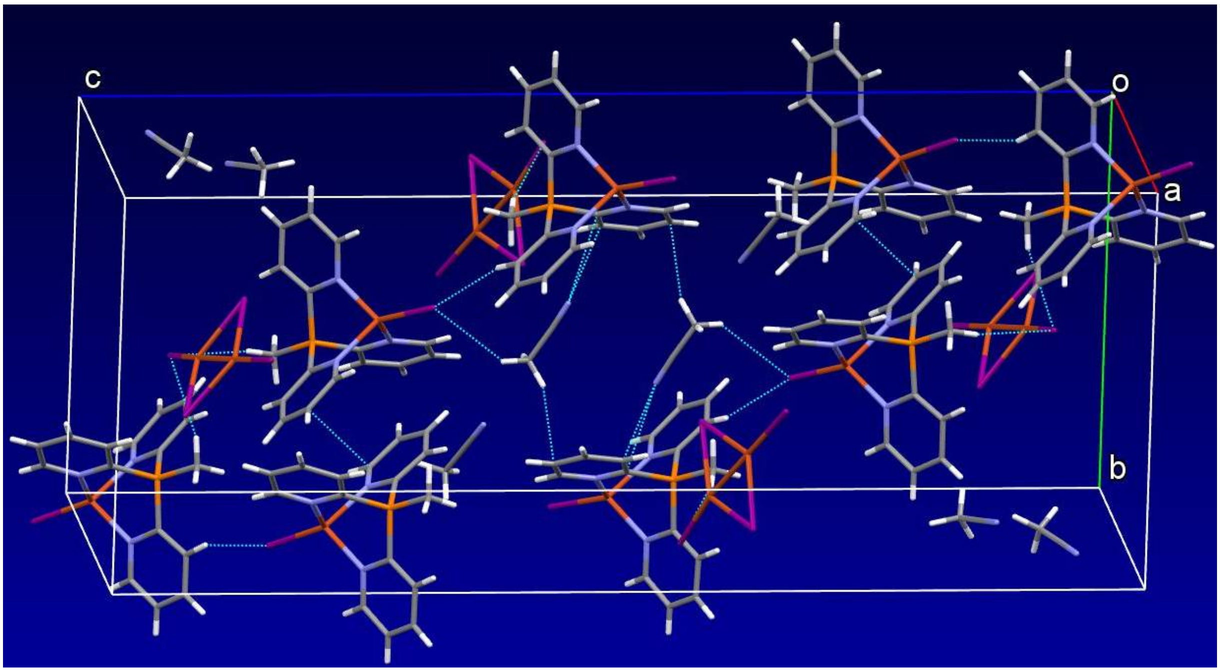

Figure S2. The crystal packing of **1**·2MeCN showing the C–H···π and C–H···I intermolecular interactions.

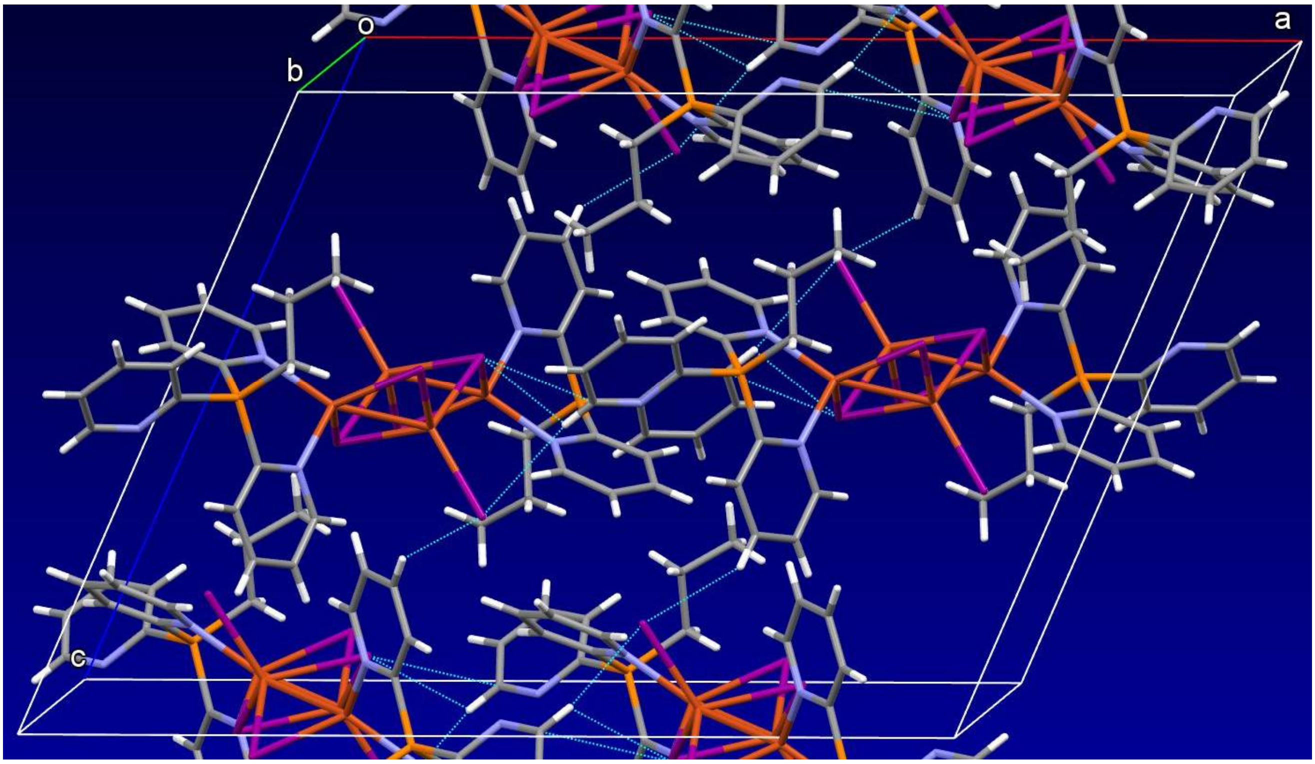

Figure S3. The crystal packing of **2** showing the C–H···I intermolecular interactions.

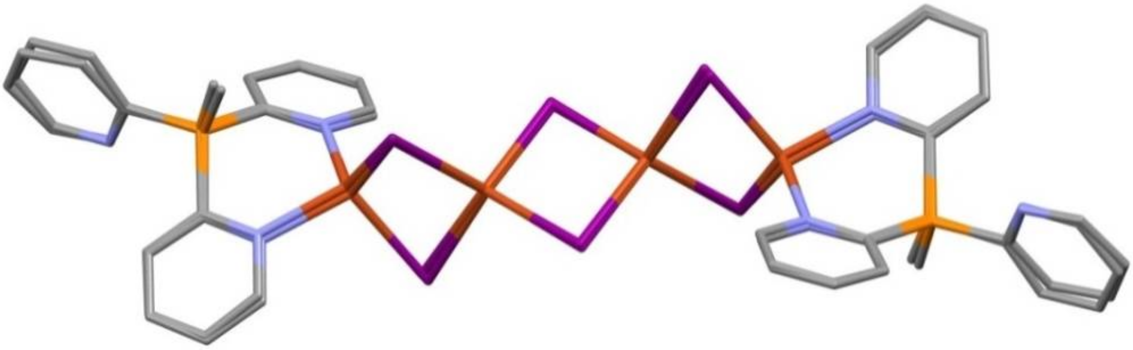

Figure S4. Overlay of the molecules of **3** and **4** (the propyl chain of **3** and phenyl group of **4** are omitted).

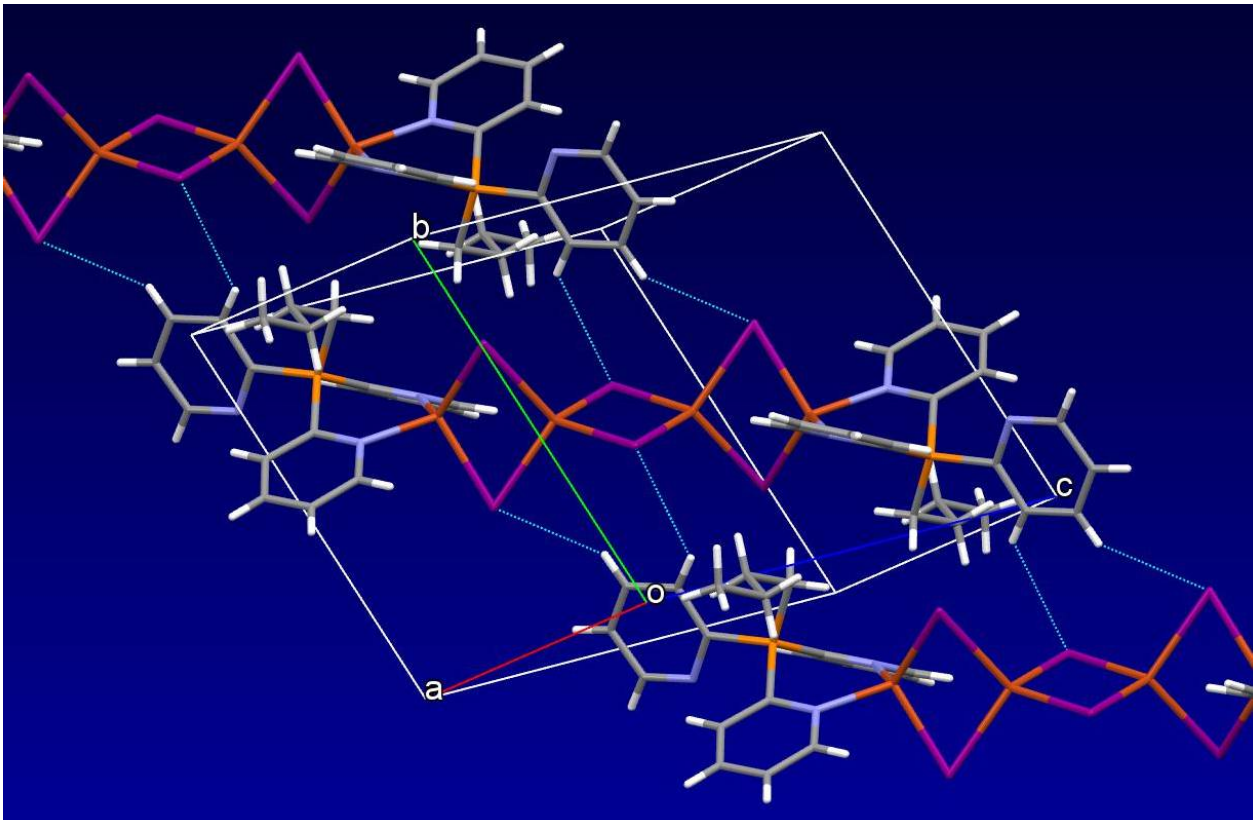

Figure S5. The crystal packing of **3** showing the C–H···I intermolecular interactions.

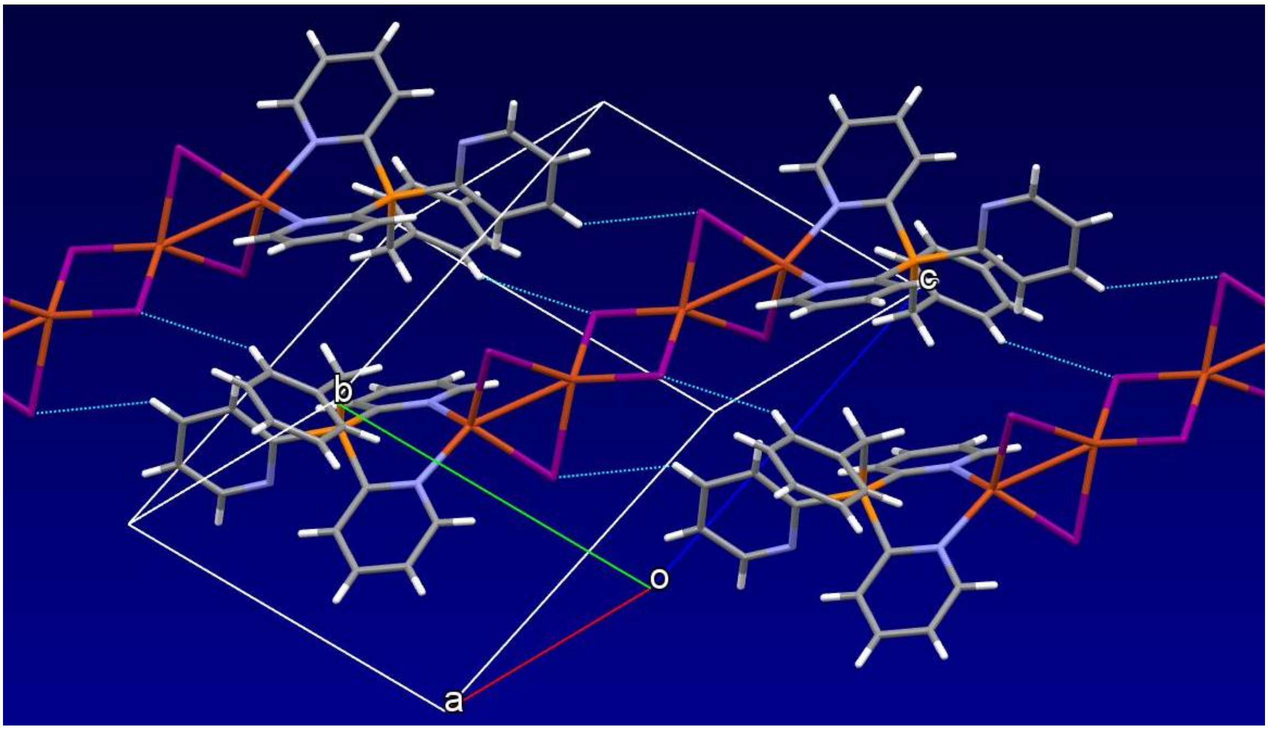

Figure S6. The crystal packing of **4** showing the C–H···I intermolecular interactions.

Table S2. Selected bonds lengths (Å) and angles (°) of the complex **2** at 200 and 296 K.

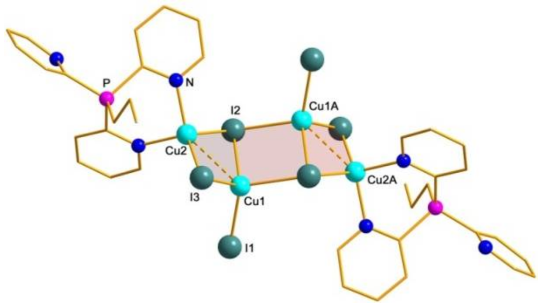

	200 K	**296 K**
Cu1 – Cu2	2.7828(5)	2.8175(7)
Cu1 – Cu1A	3.4277(5)	3.4513(9)
Cu1 – I1	2.5853(4)	2.5841(6)
I2 – Cu1 – I3	112.604(13)	111.77(2)
I2 – Cu2 – I3	117.355(12)	116.826(2)
N – Cu2 – N	96.75(8)	96.25(11)

§2. Thermogravimetry

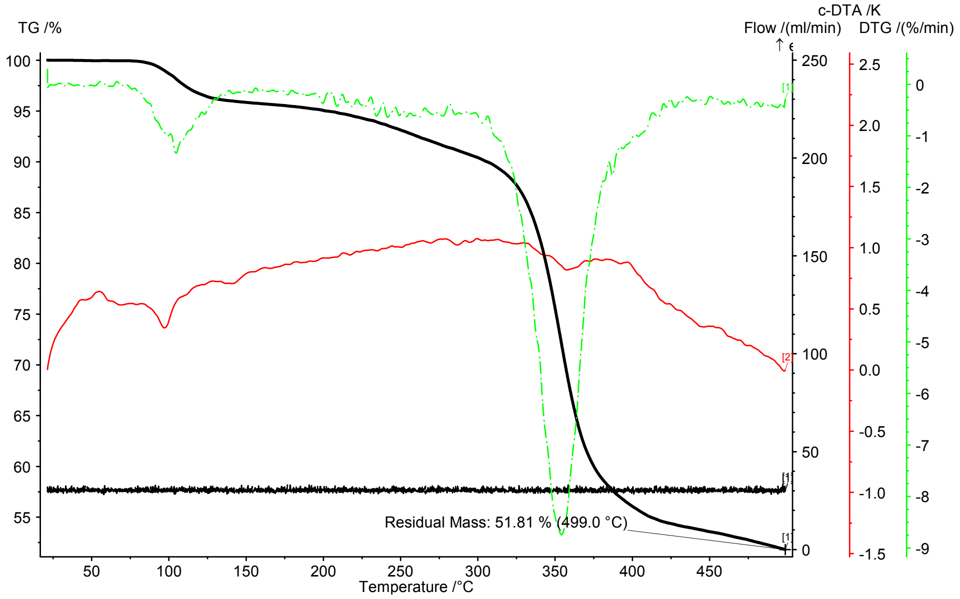

Figure S7. TG, c-DTA and DTG curves for **1**.

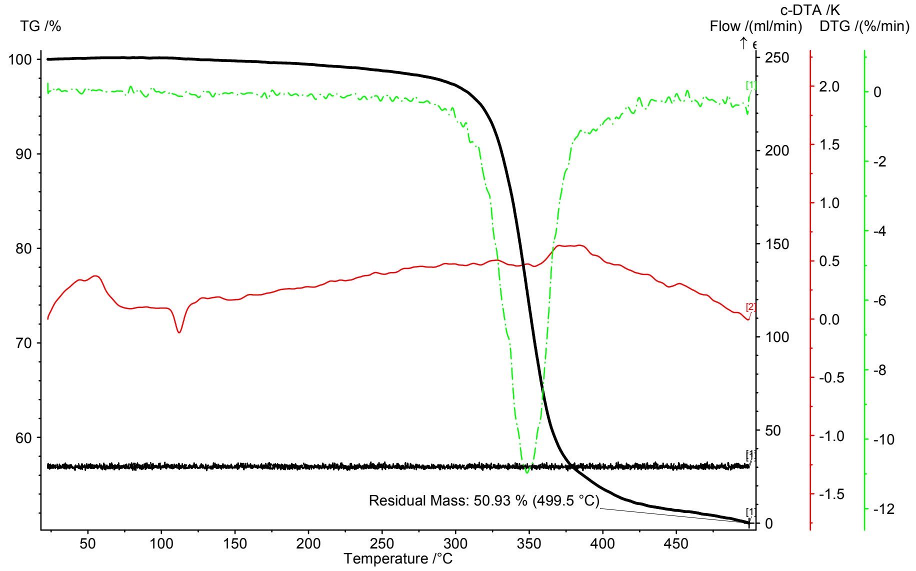

Figure S8. TG, c-DTA and DTG curves for **2**.

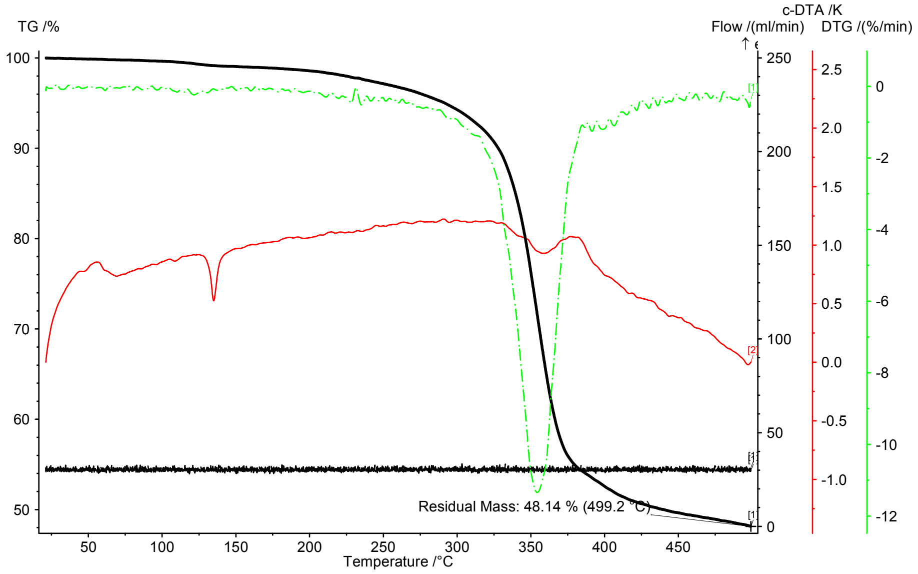

Figure S9. TG, c-DTA and DTG curves for **3**.

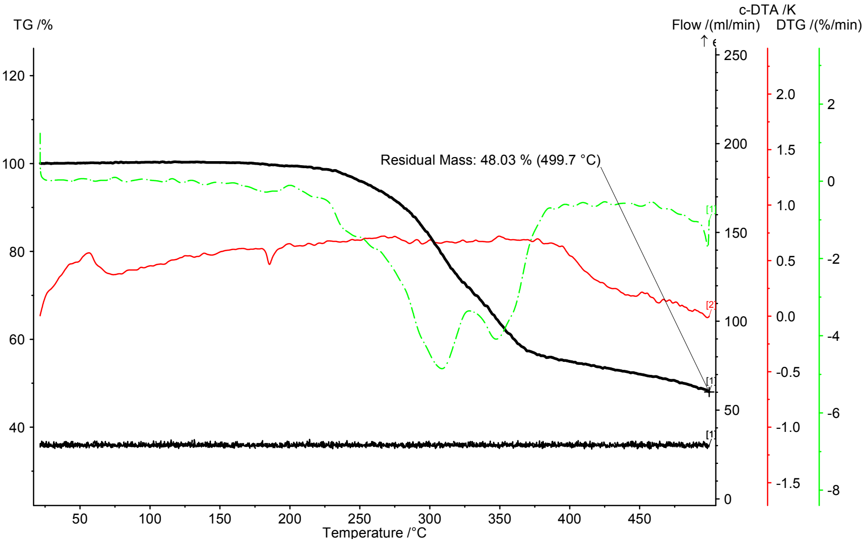

Figure S10. TG, c-DTA and DTG curves for **4**.

§3. FT-IR spectra

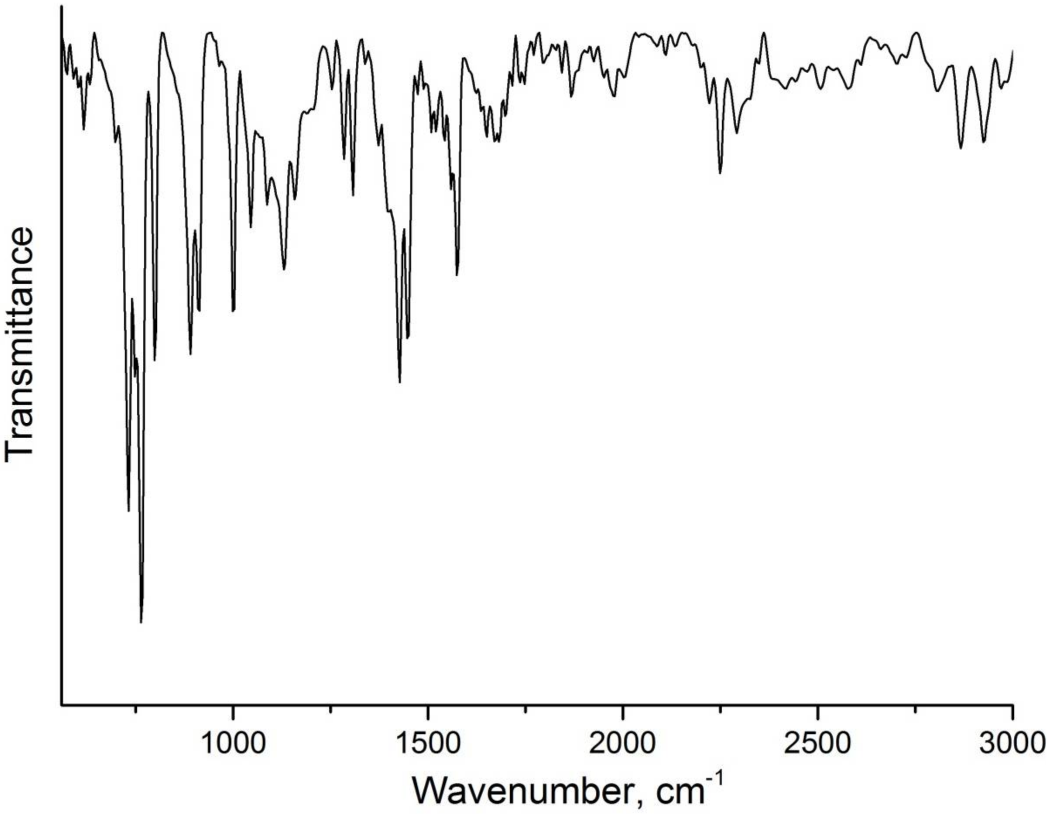

Figure S11. FT-IR spectrum of **1**.

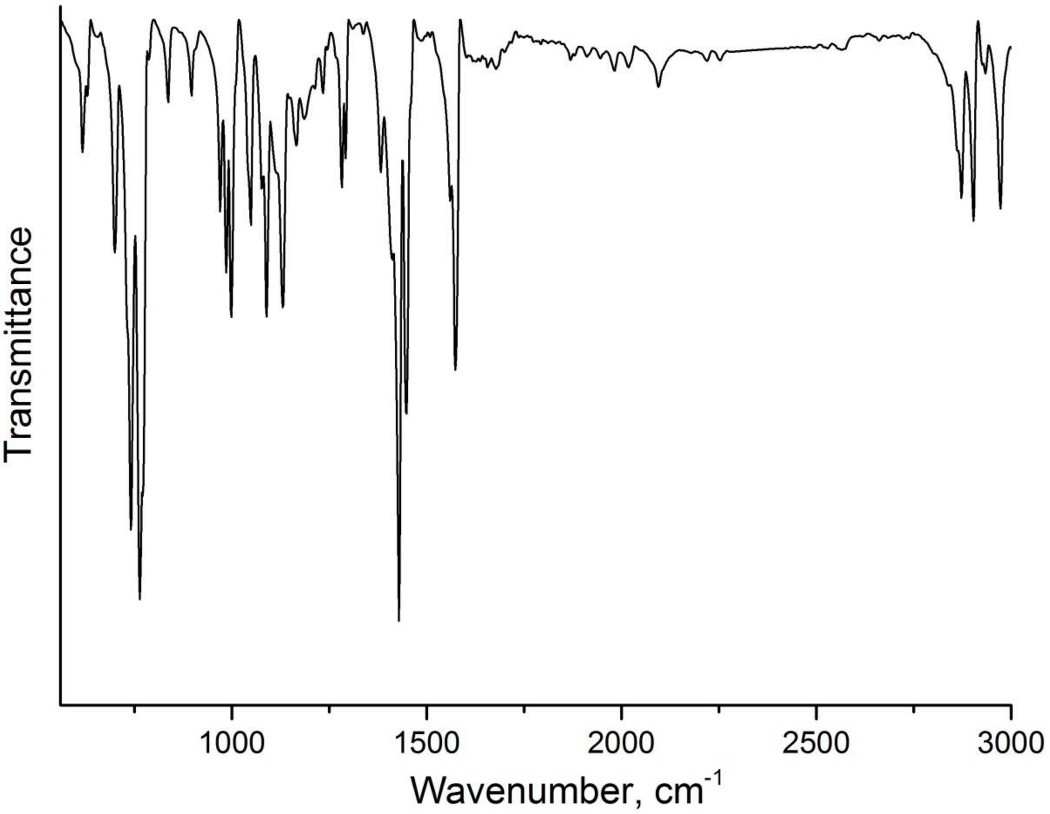

Figure S12. FT-IR spectrum of **2**.

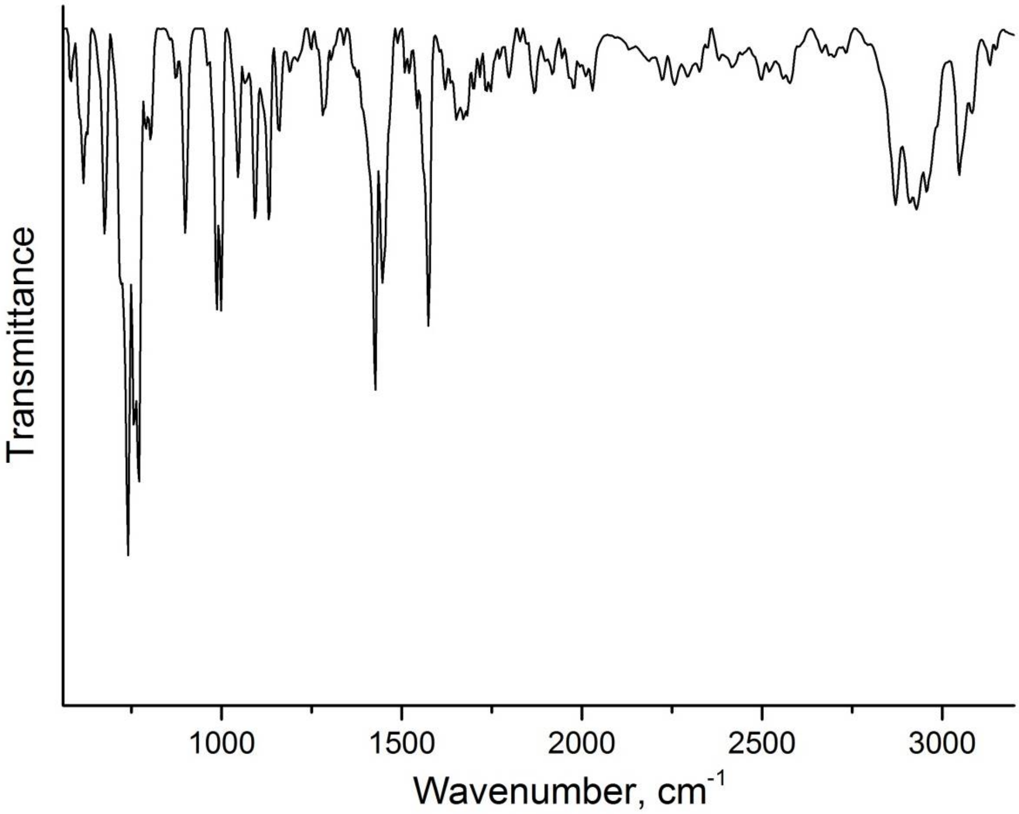

Figure S13. FT-IR spectrum of **3**.

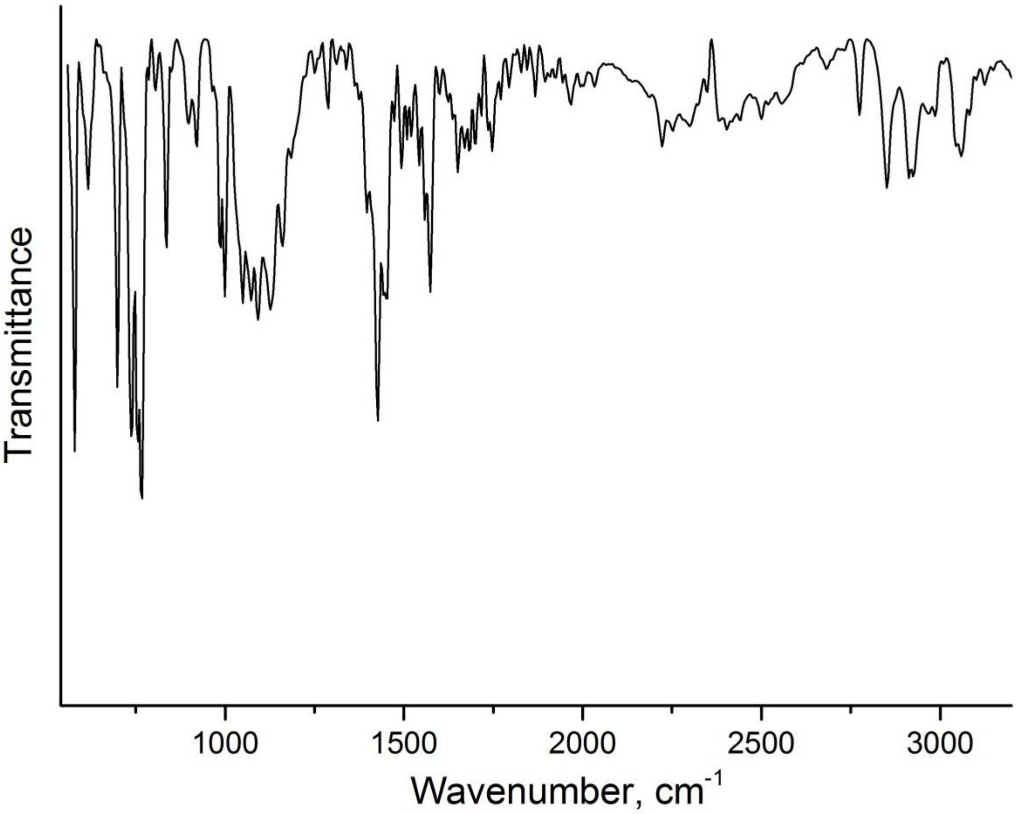

Figure S14. FT-IR spectrum of **4**.

§4. ^{1}H and ^{31}P{^{1}H} NMR spectra

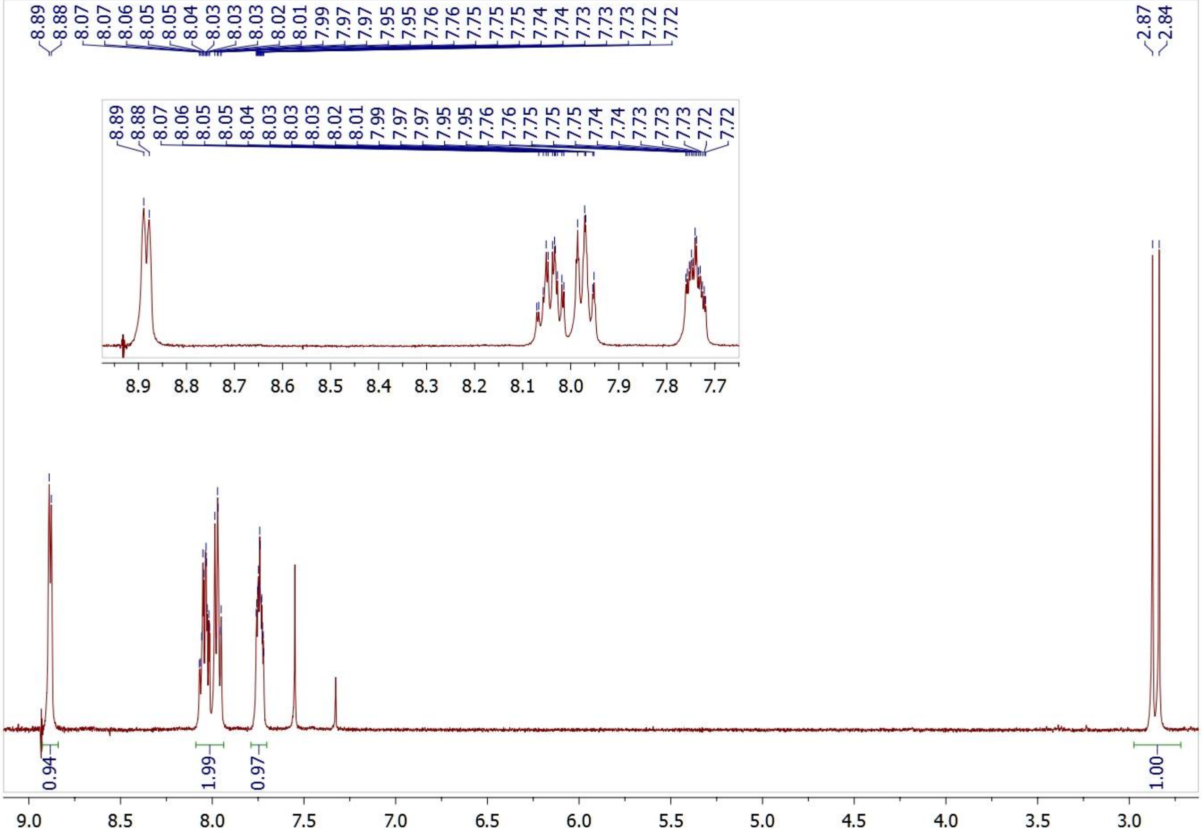

Figure S15. ^{1}H NMR spectrum of **1** (CD_3CN, 296 K).

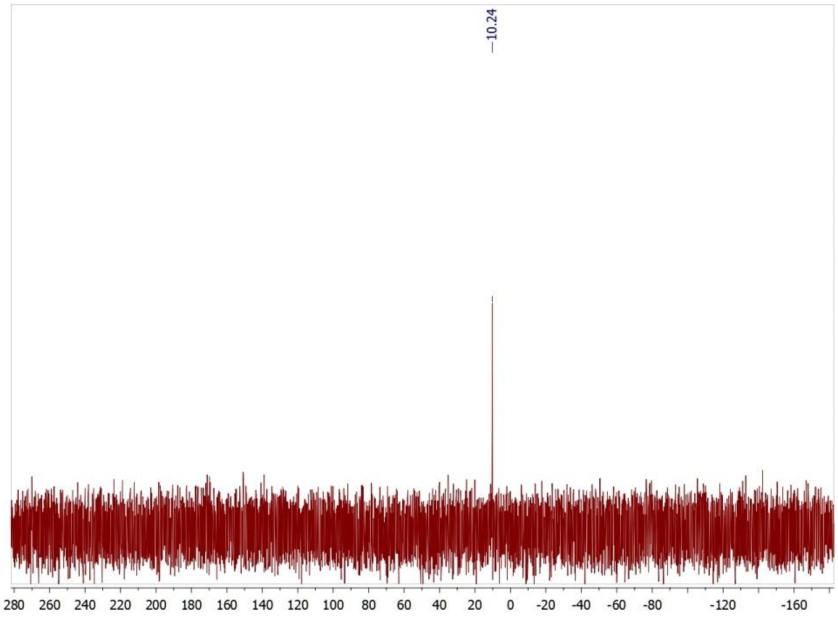

Figure S16. ^{31}P{^{1}H} NMR spectrum of **1** (CD_3CN, 296 K).

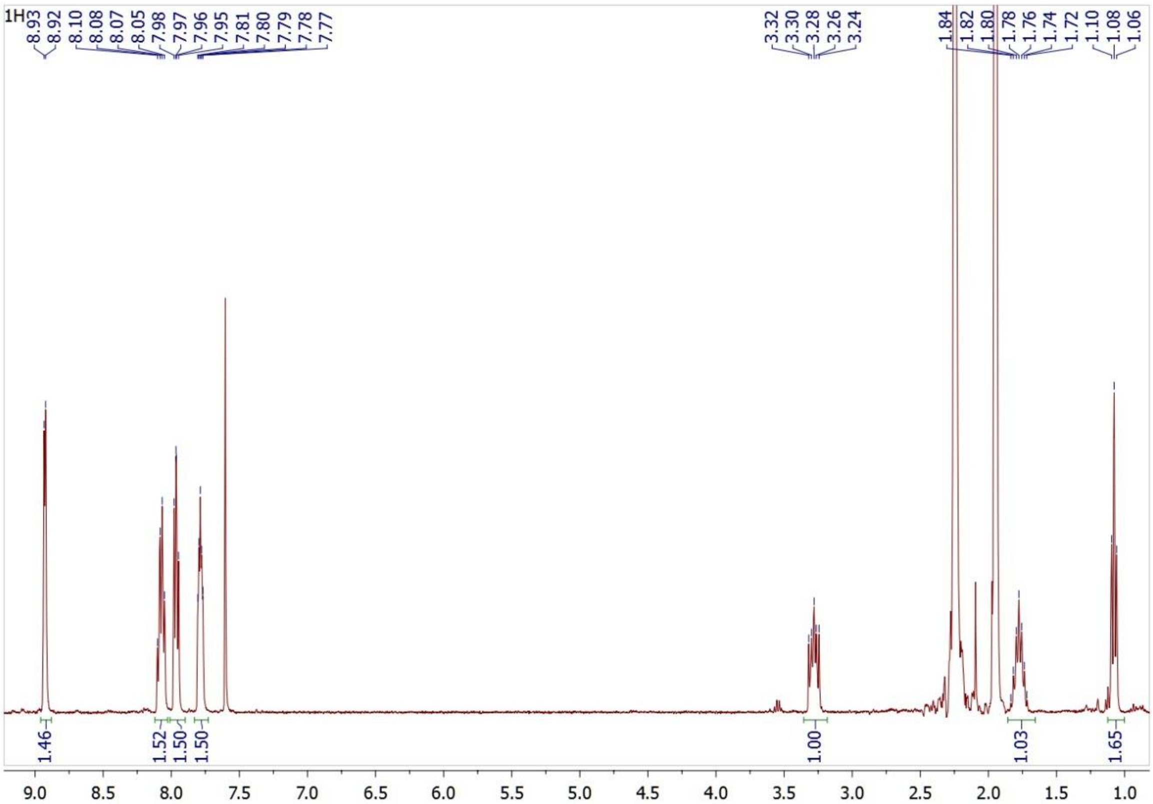

Figure S17. ^{1}H NMR spectrum of **2** (CD_3CN, 296 K).

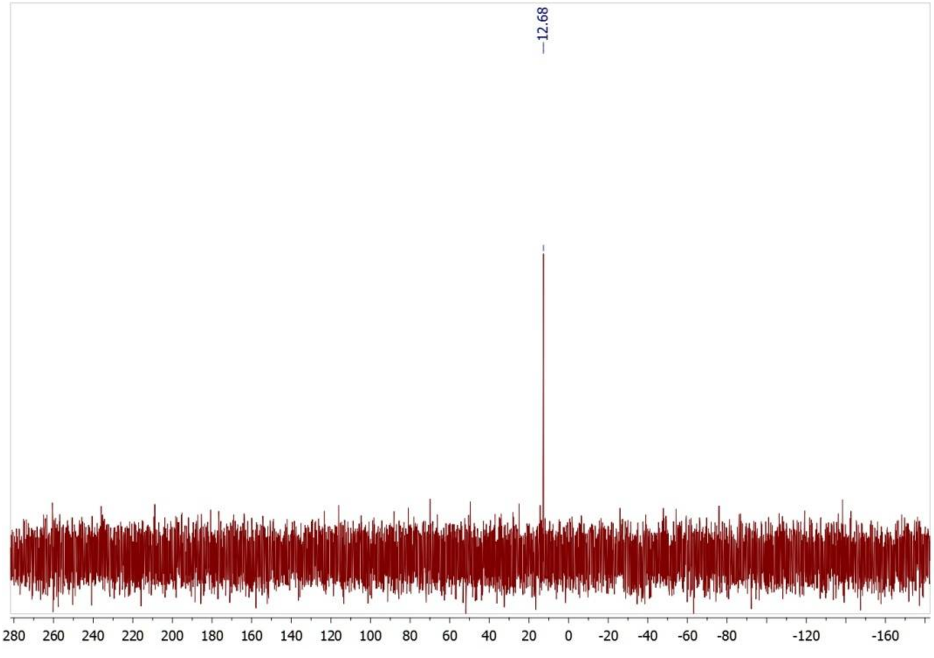

Figure S18. $^{31}P\{^{1}H\}$ NMR spectrum of **2** (CD_3CN, 296 K).

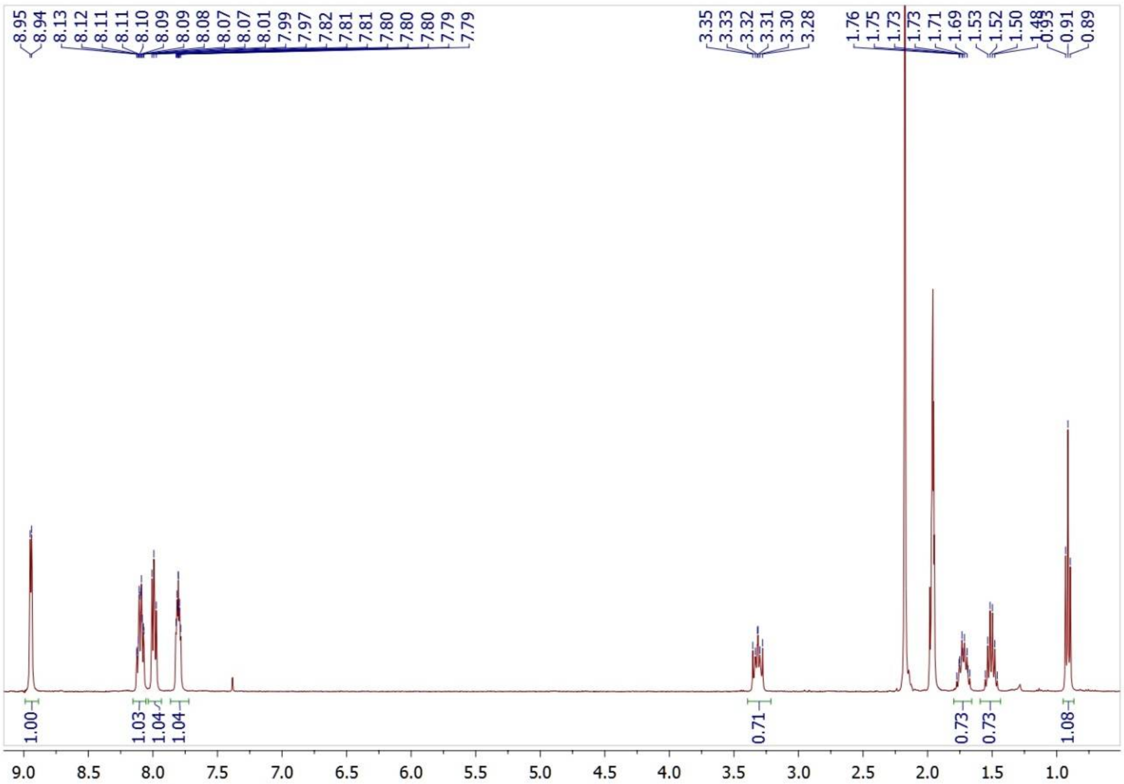

Figure S19. ^{1}H NMR spectrum of **3** (CD_3CN, 296 K).

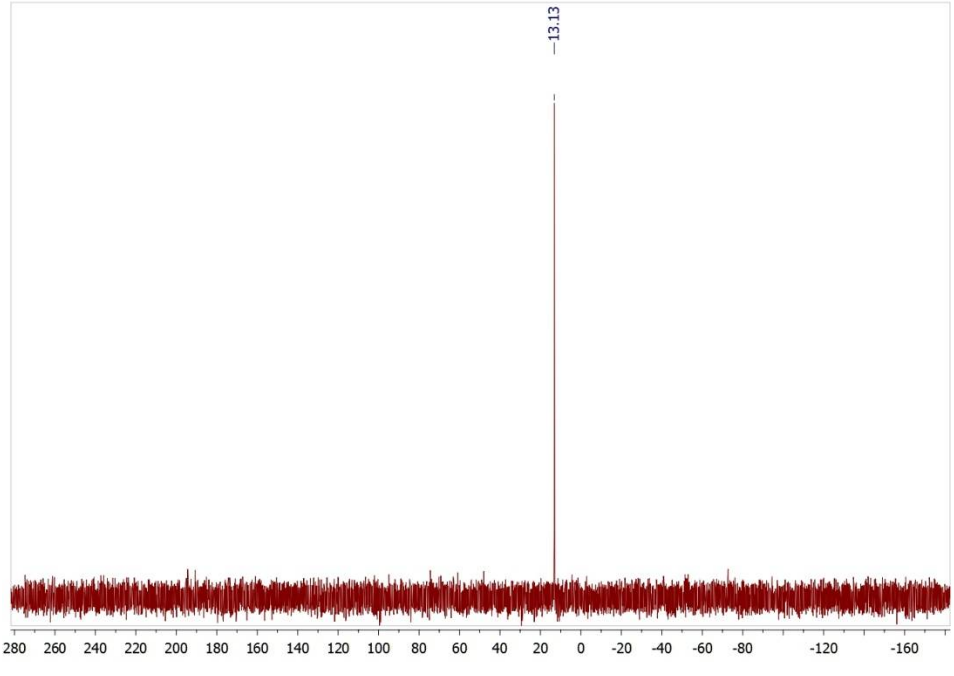

Figure S20. ^{31}P{^{1}H} NMR spectrum of **3** (CD_3CN, 296 K).

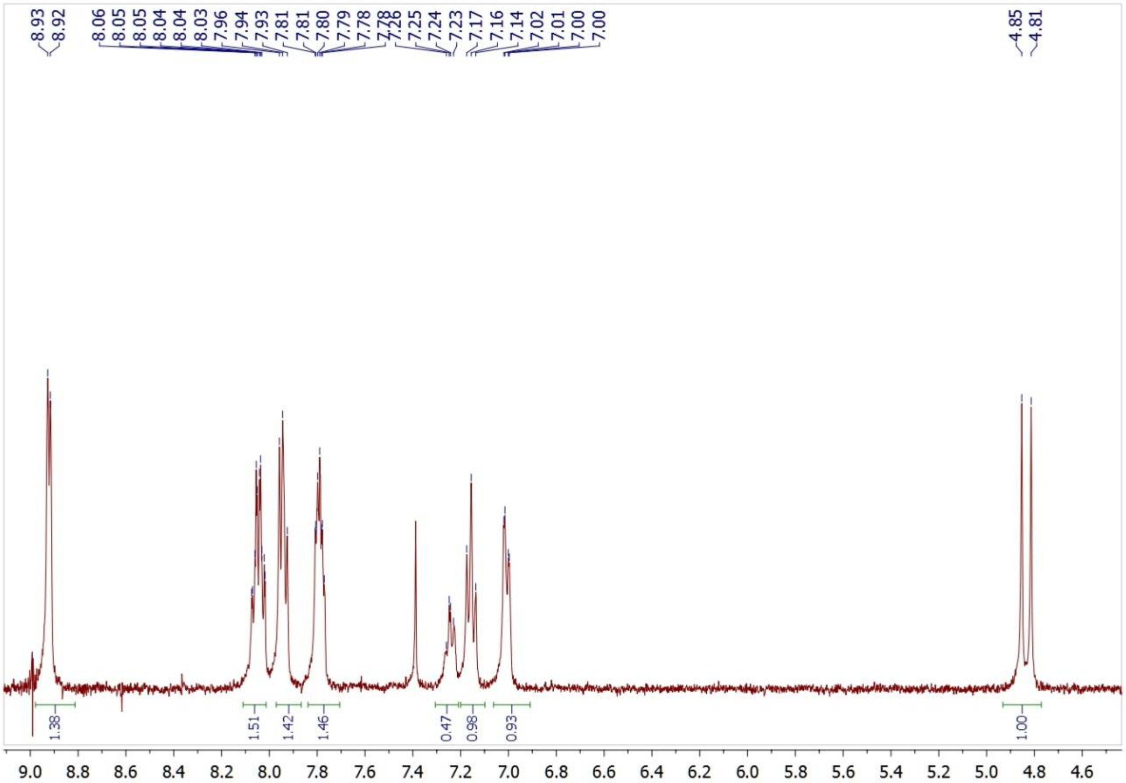

Figure S21. ^1H NMR spectrum of **4** (CD_3CN, 296 K).

§5. ESI-MS spectra

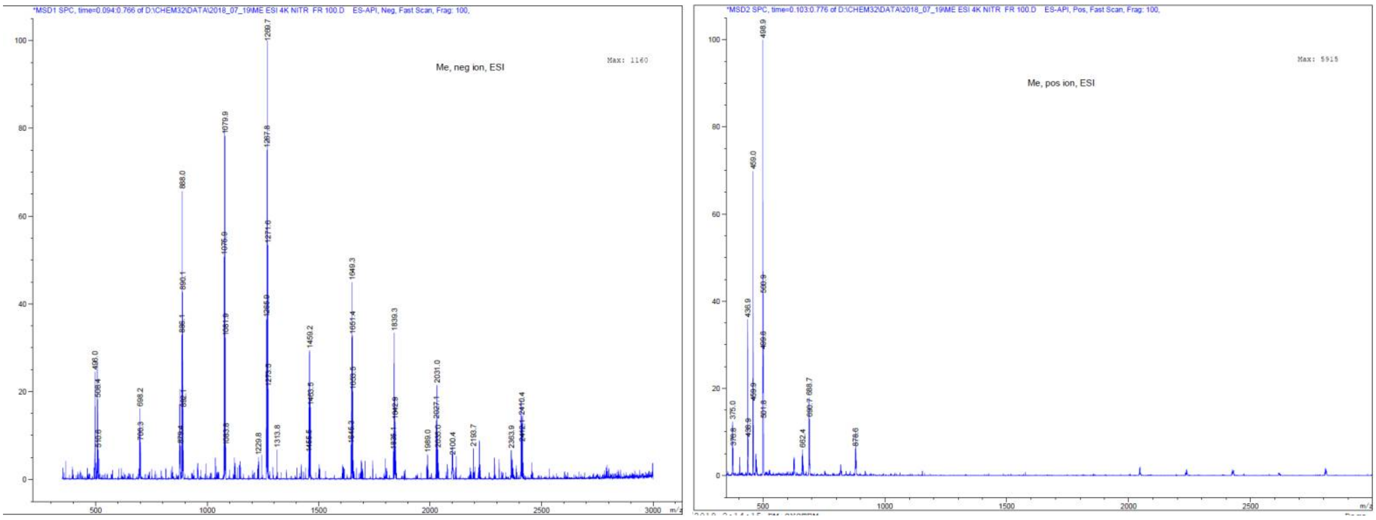

Figure S22. ESI-MS(–) (*left*) and ESI-MS(+) spectra of **1** (MeCN).

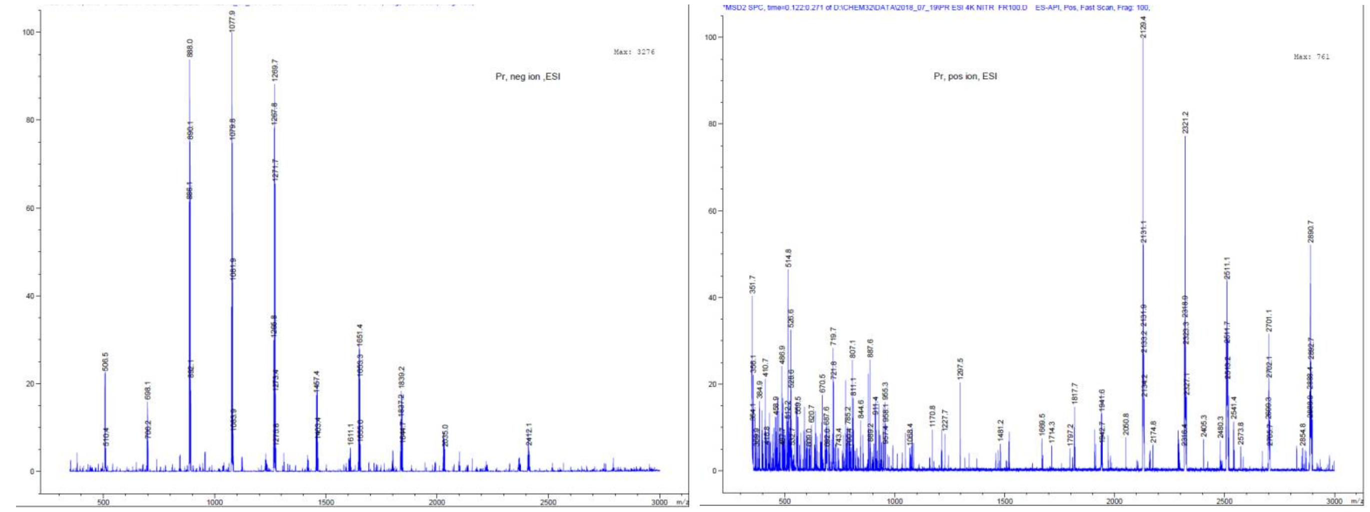

Figure S23. ESI-MS(–) (*left*) and ESI-MS(+) spectra of **2** (MeCN).

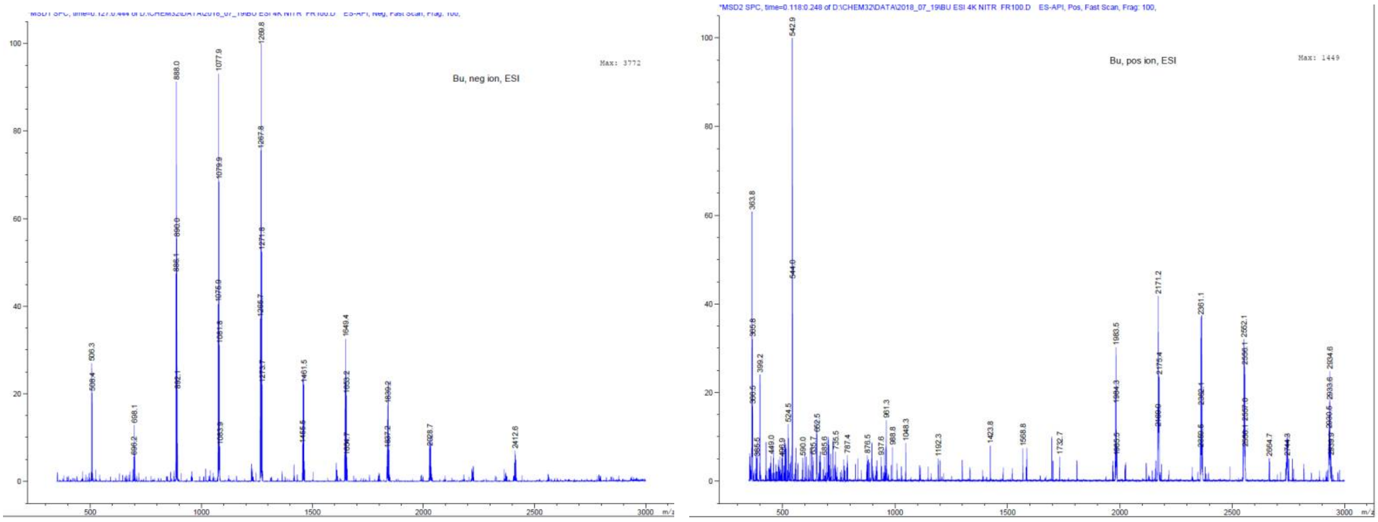

Figure S24. ESI-MS(–) (*left*) and ESI-MS(+) spectra of **3** (MeCN).

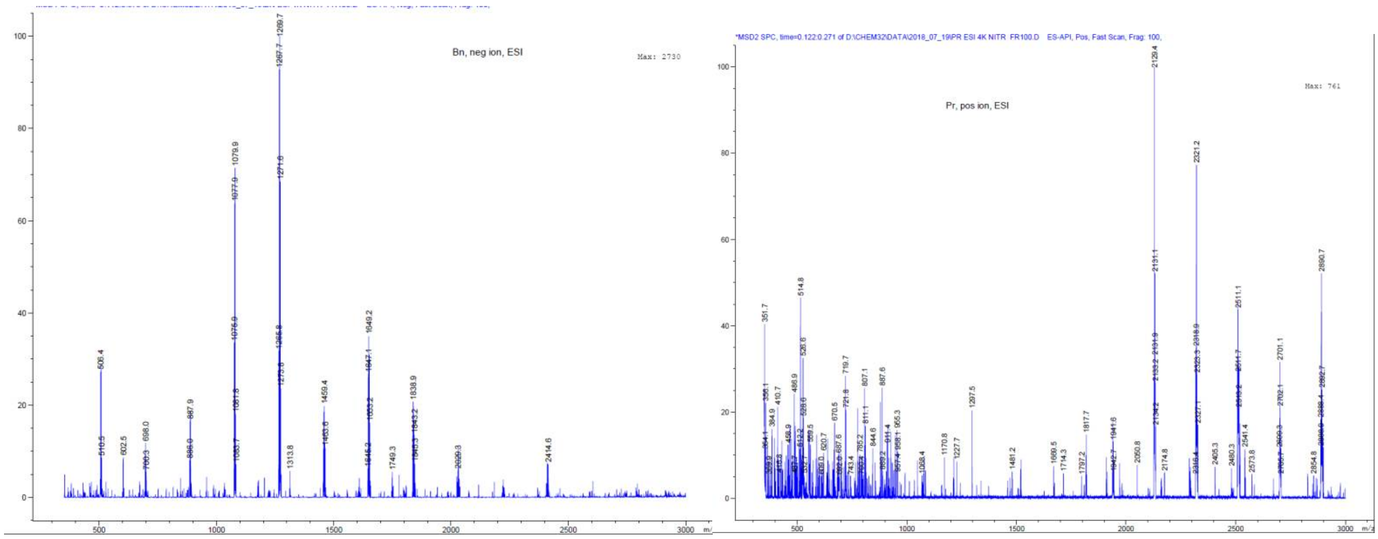

Figure S25. ESI-MS(–) (*left*) and ESI-MS(+) spectra of **3** (MeCN).

§6. Photophysical data

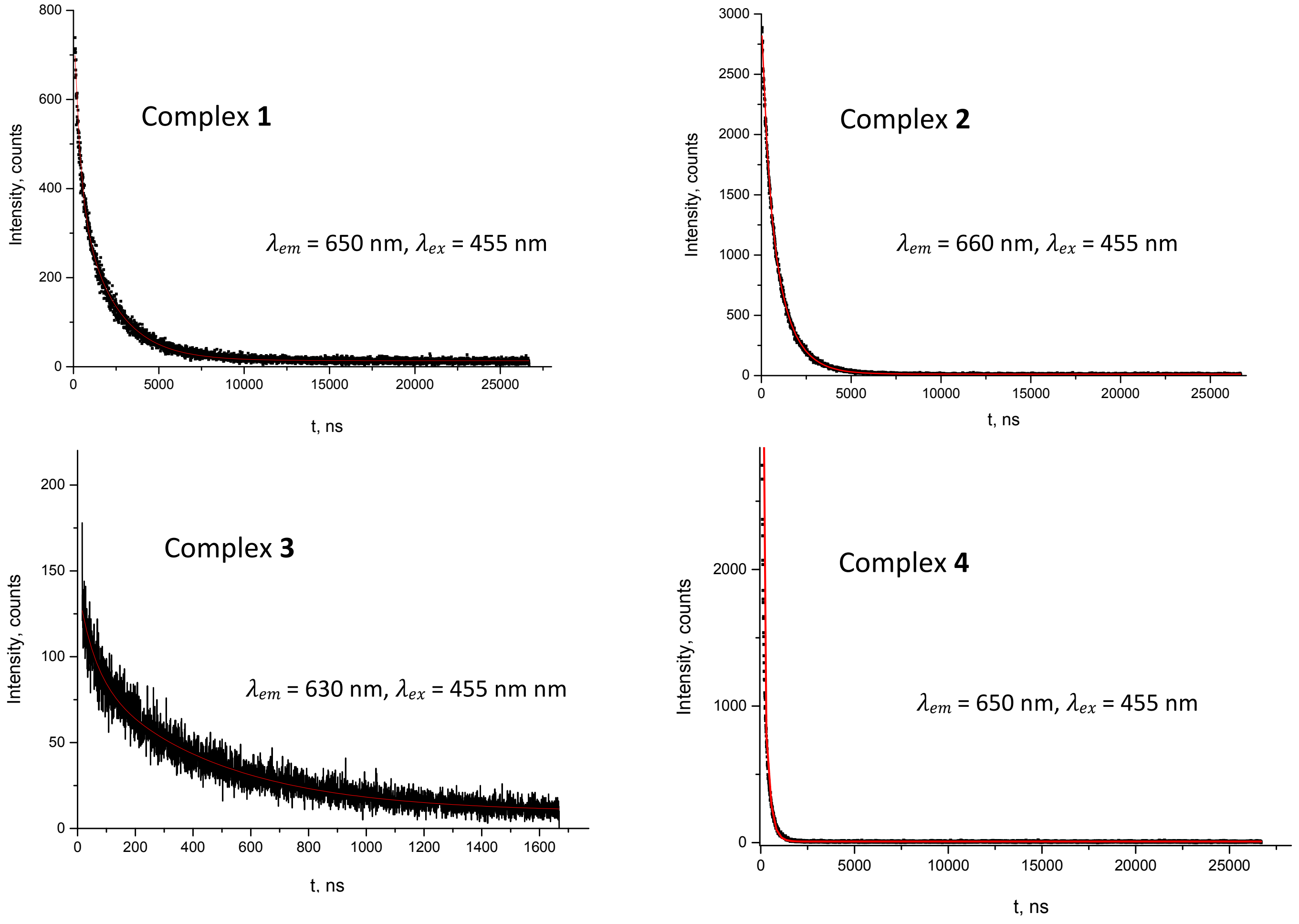

Figure S26. Emission decay for complexes **1**–**4** in the solid state at 296 K.

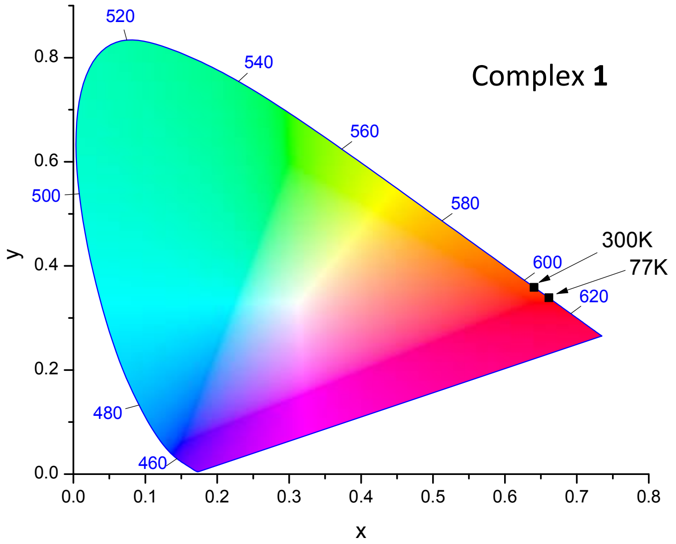

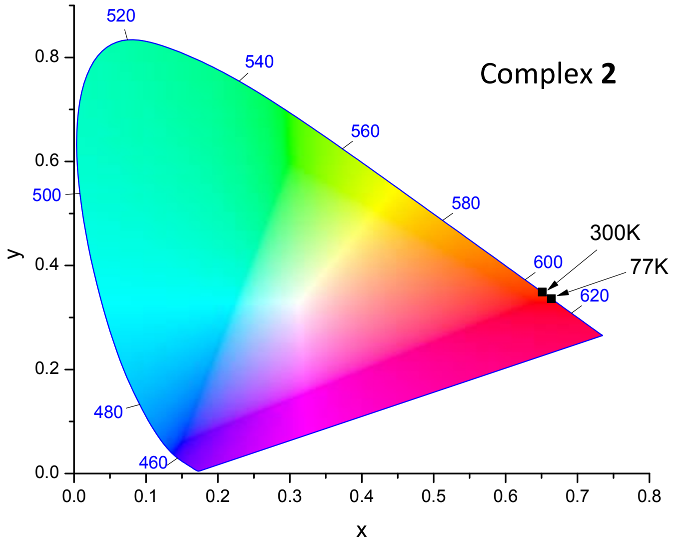

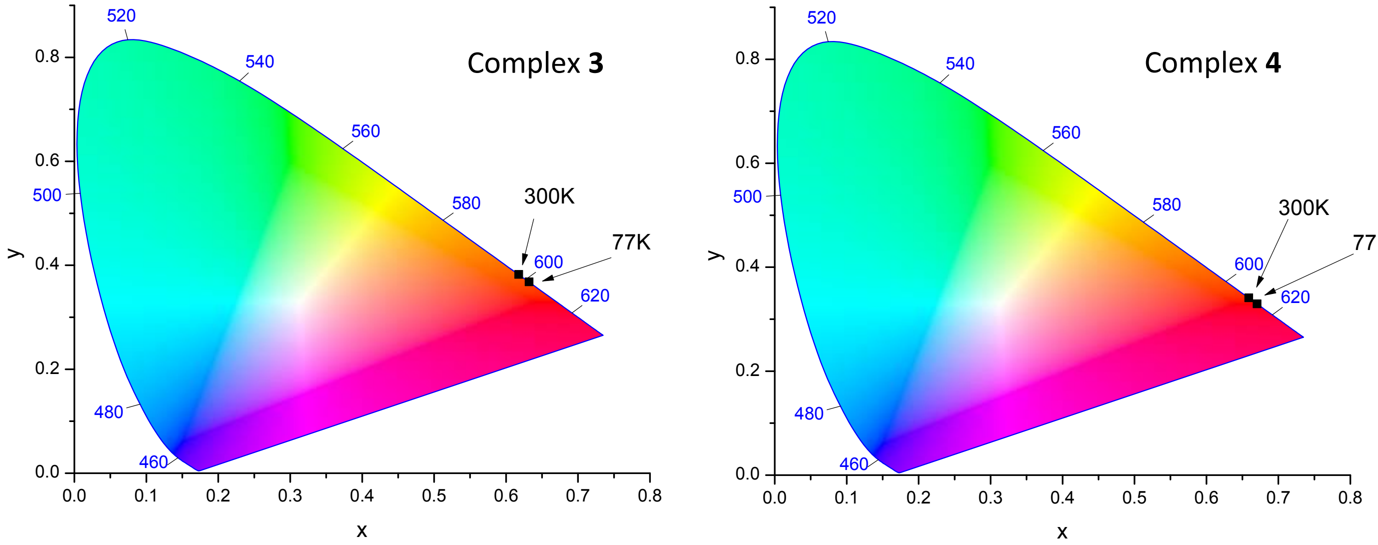

Figure S27. CIE chromaticity diagrams showing the temperature dependence of the color coordinates for **1**–**4** (λ_{ex} = 450 nm).

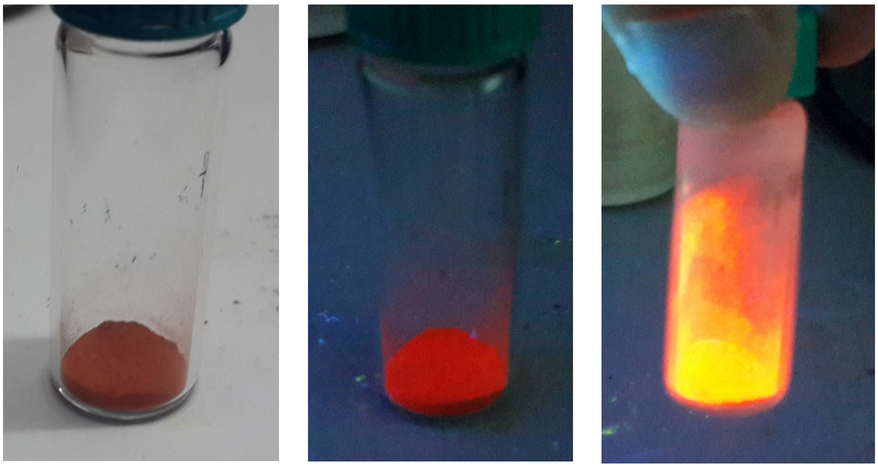

(*a*) (*b*) (*c*)

Figure S28. The powder of **4**: under day-light at 298 K (*a*); under 350 nm light at 300 K (*b*) and about 100 K (*c*).

§7. Computational details

The solid-state UV-Vis spectra calculated from the diffuse reflectance data applying a Kubelka–Munk function are usually coincide fairly well with the spectra recorded in solution. Although it should be noted that the solid-state spectra are less resolved and characterized by the extended tails of the long-wavelength bands.[1] Therefore, to analyze the solid-state UV-Vis spectra of complexes **1**–**4**, we performed time-dependent (TD) DFT calculations[2] for isolated complexes with the their XRD geometries. To simplify calculations, the propyl or butyl substituents in phosphonium cation and one of the pyridine rings, not involved in the coordination by Cu(I), were replaced by hydrogen atom and methyl group, respectively.

It is well-known,[2,3] that TD-DFT approach with GGA (e.g. BP86[4]) or hybrid (e.g. B3LYP[5]) functionals underestimates significantly the energies of the charge-transfer (CT) states. A series of special functionals (e.g. long-range corrected CAM-B3LYP[6] and LC-ωPBE,[7] meta-GGA M06-HF,[8] and double-hybrid B2PLYP[9]) were proposed to solve this problem. Thus, we employed the latter functionals, as well as BP86 and B3LYP for comparison, to calculate the maxima and oscillator strengths in the UV-Vis spectra of complexes **1**–**3**. Basis sets of def2-TZVP quality[10] (with relativistic effective core potential, ECP, for iodine) were used in the calculations. For calculations at the TD-BP86, TD-B2PLYP levels, the ORCA suit of programs[11] has been employed. For all other calculations, the GAUSSIAN09 suit of programs[12] has been used.

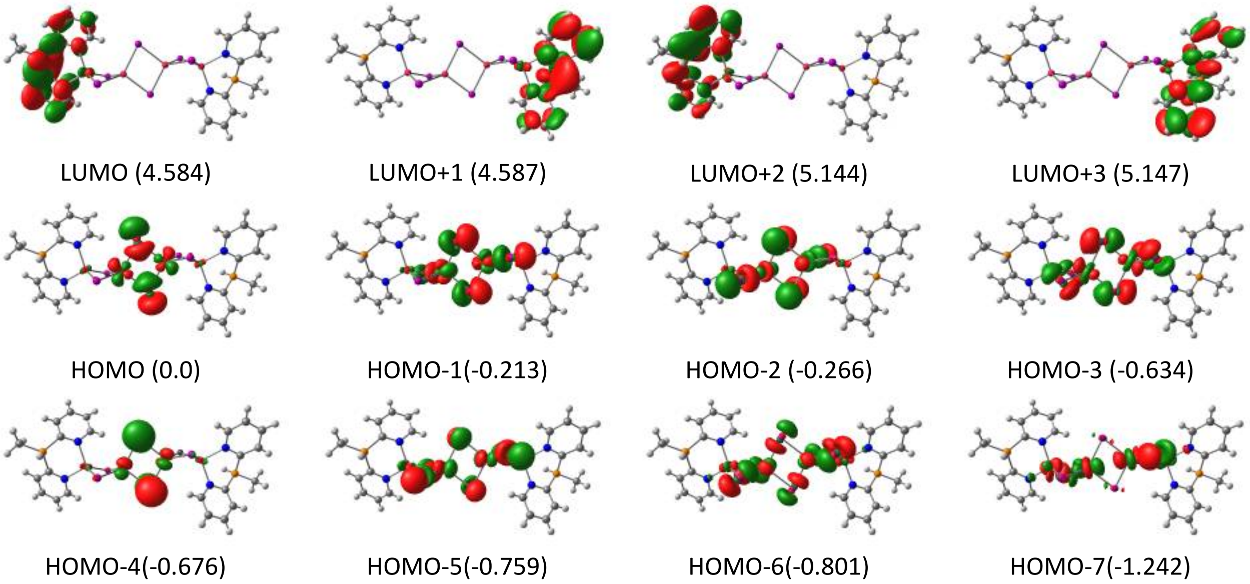

LUMO (4.584) LUMO+1 (4.587) LUMO+2 (5.144) LUMO+3 (5.147)

HOMO (0.0) HOMO-1(-0.213) HOMO-2 (-0.266) HOMO-3 (-0.634)

HOMO-4(-0.676) HOMO-5(-0.759) HOMO-6(-0.801) HOMO-7(-1.242)

Figure S29. Four lowest unoccupied and 8 highest occupied MOs for complex **3** calculated at the LC-ωPBE/def2-TZVP level, relative MO energies in eV are presented in parenthesis.

We did not perform calculations for complex **4**, as it has chemical structure and properties very similar to those of complex **3**. The case of complex **3** is a representative. For all methods employed, we calculated energies and oscillator strengths for 50 lowest-energy electronic transitions. For complex **3**, all these transitions had a CT nature. Figure S29 represents a series of MOs for this complex calculated at the LC-ωPBE/def2-TZVP level.

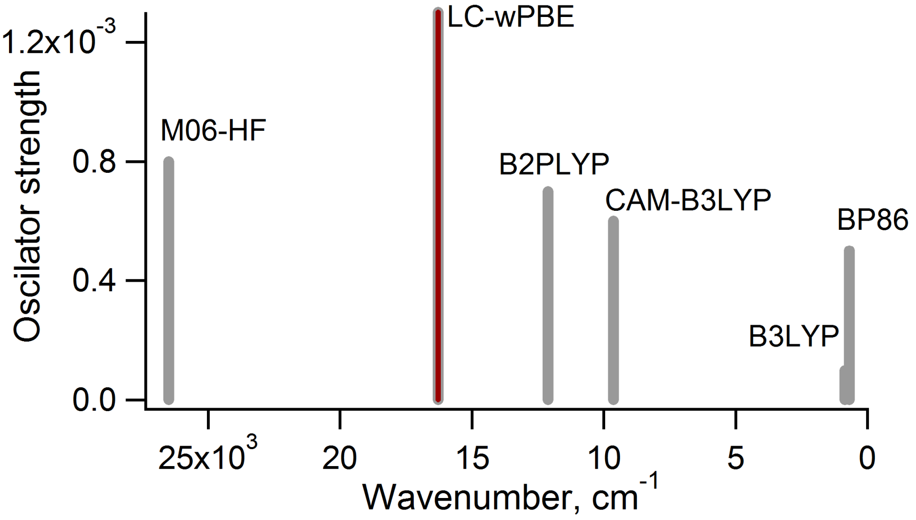

Figure S30. Positions and oscillator strengths of the long-wavelength transition in the electronic absorption spectrum of complex **3** calculated using TD-DFT/def2-TZVP method with different functionals.

Figure S30 demonstrates that application of both the BP86 and B3LYP functionals leads to unreasonably low energy of the long-wavelength transition (~0.1 eV). All functionals specially designed to improve the accuracy of predicting the CT-transition energies lead to significantly higher energy in a wide range of 1.2 – 3.3 eV. Comparison with experiment demonstrated that only calculations with LC-ωPBE functional reproduce fairly well experimental UV-Vis spectrum although the energies of CT states are still slightly underestimated (Fig. S31). Wherein, calculations with CAM-B3LYP and B2PLYP functionals significantly underestimate the CT-state energies, while calculations with M06-HF functional even overestimate tremendously these energies.

The computed electronic absorption spectrum of complex **3** in the near-UV and visible region (Fig. S31, dashed line) represents a set of CT-bands corresponding to the electron promotions from the MOs localized on the $[Cu_4I_6]^{2-}$ cluster (composed of the iodine p-orbitals and Cu(I) d-orbitals) to the MOs localized mainly on the pyridine rings of the cations.

All unoccupied MOs involved in these transitions represents pairs of close-energy orbitals localized on two different ligands (e.g. see Fig. S29). Thus, all CT transitions also represent pairs with similar energy but different oscillator strengths (f). For example, pair of long-wavelength transitions for **3** was predicted at 614.1 and 613.9 nm with f = 0.0013 and 0.0062. The first transition is originated from a number of electron promotions from a series of occupied MOs (HOMO-1, HOMO-3, HOMO-6, HOMO-7) to LUMO+1, and the second transition is mainly originated from the electron excitations from the same MOs and HOMO to the LUMO. The most intense transition at 562 nm (f=0.0619) and its partner at 561.3 nm (f=0.0008) are also originated from the electron excitations to LUMO and LUMO+1. Moreover, we calculated energies of the first triplet excited states at the geometry of the ground state. The energy difference between lowest singlet and triplet excited states was predicted to be small enough [e.g. $\Delta E(S_1–T_1) = 1137\ cm^{-1}$] making possible the manifestation of thermally activated delayed fluorescence (TADF).[13]

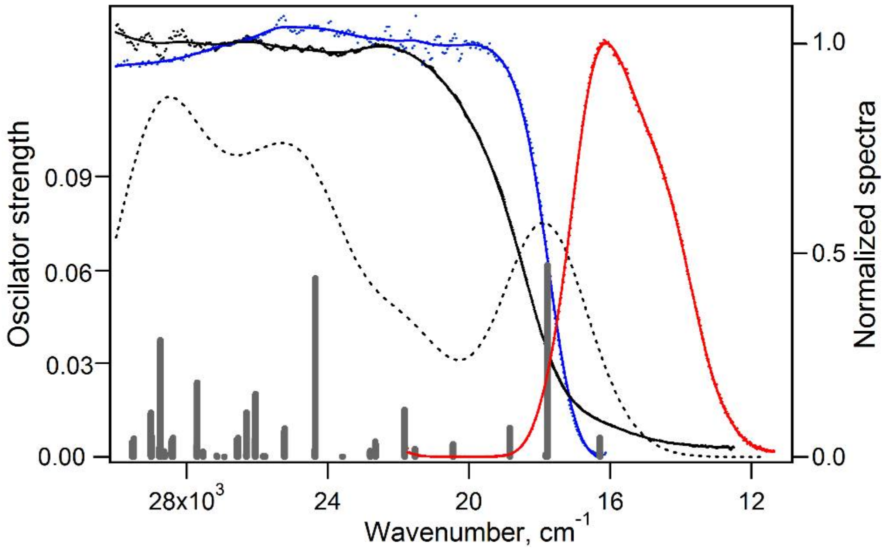

Figure S31. The solid-state normalized spectra for complex **3** at 298 K: Kubelka-Munk function (black solid), photoluminescence (λ_{ex} = 455 nm, red) and luminescence excitation (blue) spectra. Vertical black bars indicate the positions and oscillator strengths (f, left axis) of the electronic transitions calculated at the LC-ωPBE/def2-TZVP level for isolated complex **3** with XRD geometry. For convenience, a theoretical absorption spectrum of complex **3** computed applying 4000 cm^{-1} Gaussian broadening of the individual transitions (black bars) is also presented (dotted line).

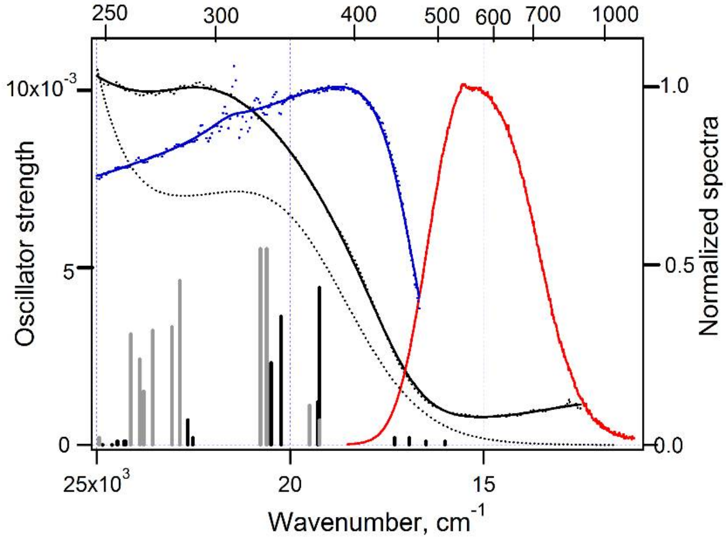

Figure S32. The solid-state normalized spectra for compound **1** at 298 K: Kubelka-Munk function (black solid), photoluminescence (λ_{ex} = 455 nm, red) and luminescence excitation (blue) spectra. Vertical black bars indicate the positions and oscillator strengths (f, left axis) of the electronic transitions calculated at the LC-ωPBE /def2-TZVP level for isolated compound **1**. For convenience, a theoretical absorption spectrum of **1** computed applying 4000 cm^{-1} Gaussian broadening of the individual transitions (black bars) is also presented (dotted line).

As only long-range corrected LC-ωPBE functional performed well in the calculation of the UV-Vis spectrum of complex **3**, we used the same functional to calculate spectroscopic properties of complexes **2** and **1**. Results of calculations for complex **2** are presented in the main text.

Figure 7 (main text) shows that all complexes **1**–**4** have similar UV-Vis spectra although complex **1** contains well separated cations {$[Cu(Me\text{-}TPP)I]^{+}$} and anionic cluster {$[Cu_2(\mu\text{-}I)_2I_2]^{2-}$}. Unexpectedly, calculations predict (black bars, Fig. S32) that the long-wavelength transitions of complex **1** are also originated from the electron promotions from the MOs localized on the cluster $[Cu_2I_4]^{2-}$ to the MOs localized mainly on the ligand of the $[Cu(Me\text{-}PPy_3)I]^{+}$ cation despite of large distance between dianion and cations [(r(Cu1…Cu3) = 6.76 Å, r(Cu2…Cu4) = 6.636 Å)]. In contrast to compounds **2**–**4**, more intense transitions of **1** in the visible region (grey bars) are due to the excitations localized on cations.

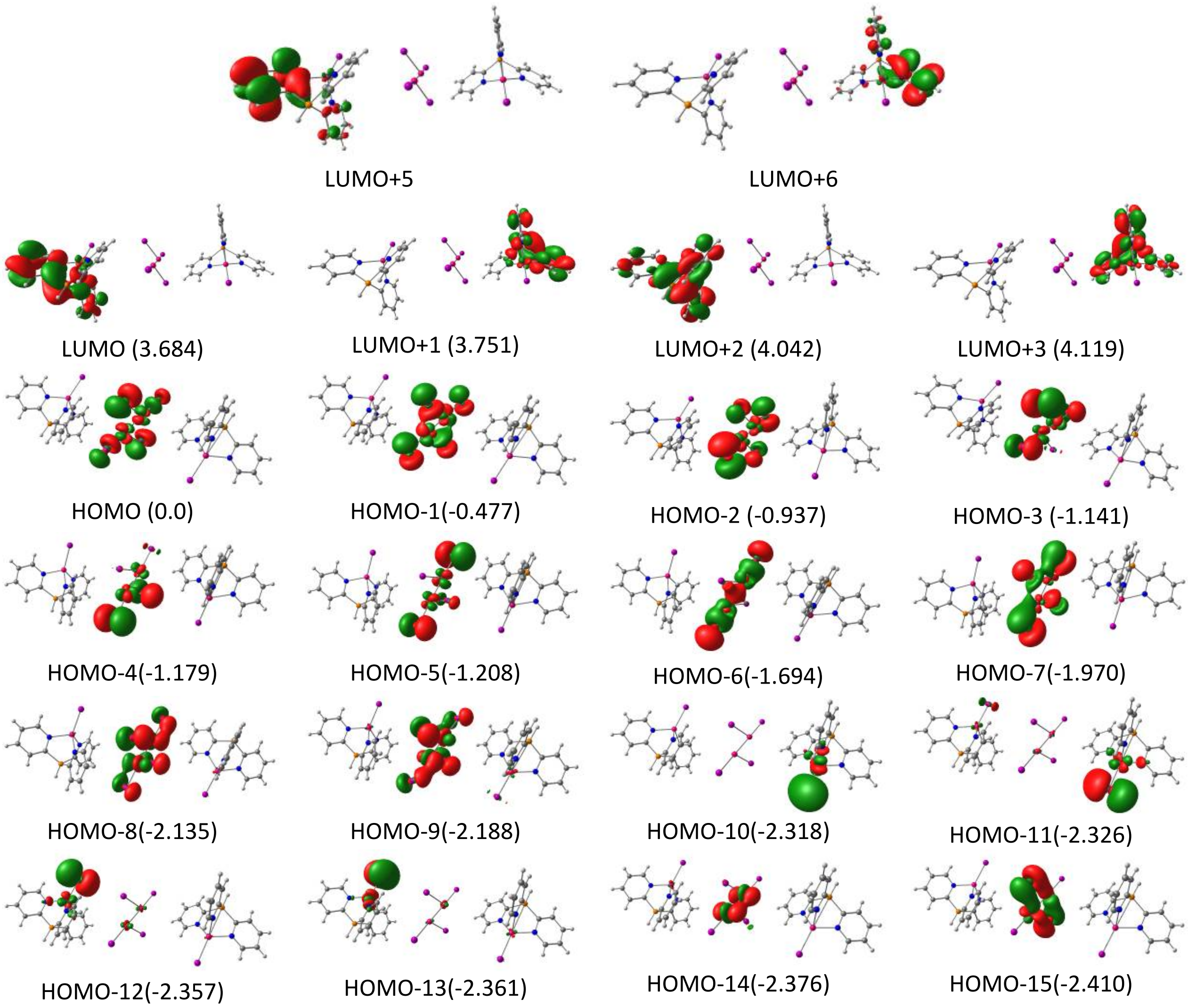

LUMO+5 LUMO+6

LUMO (3.684) LUMO+1 (3.751) LUMO+2 (4.042) LUMO+3 (4.119)

HOMO (0.0) HOMO-1(-0.477) HOMO-2 (-0.937) HOMO-3 (-1.141)

HOMO-4(-1.179) HOMO-5(-1.208) HOMO-6(-1.694) HOMO-7(-1.970)

HOMO-8(-2.135) HOMO-9(-2.188) HOMO-10(-2.318) HOMO-11(-2.326)

HOMO-12(-2.357) HOMO-13(-2.361) HOMO-14(-2.376) HOMO-15(-2.410)

Figure S33. Six lowest unoccupied and 16 highest occupied MOs for complex **1** calculated at the LC-ωPBE/def2-TZVP level, relative MO energies in eV are presented in parenthesis.

Figure S33 shows a set of MOs involved in the transitions presented in Figure S32. Transitions displayed as black bars are due to the combinations of electron excitations from occupied orbitals HOMO – (HOMO-9) to the LUMO – LUMO +6 (CT states). In turn, transitions displayed as grey bars are originated from electron excitations from MOs localized on the cations and composed mainly of iodine p-orbitals and Cu d-orbitals [e.g. (HOMO-10) – (HOMO-13), Fig. S33]. Surprisingly, but among 50 lowest-energy transitions (up to 29000 cm^{-1} or 345 nm) calculated for compound **1** at the LC-ωPBE level we did not find any cluster-centered (*CC) excitations.

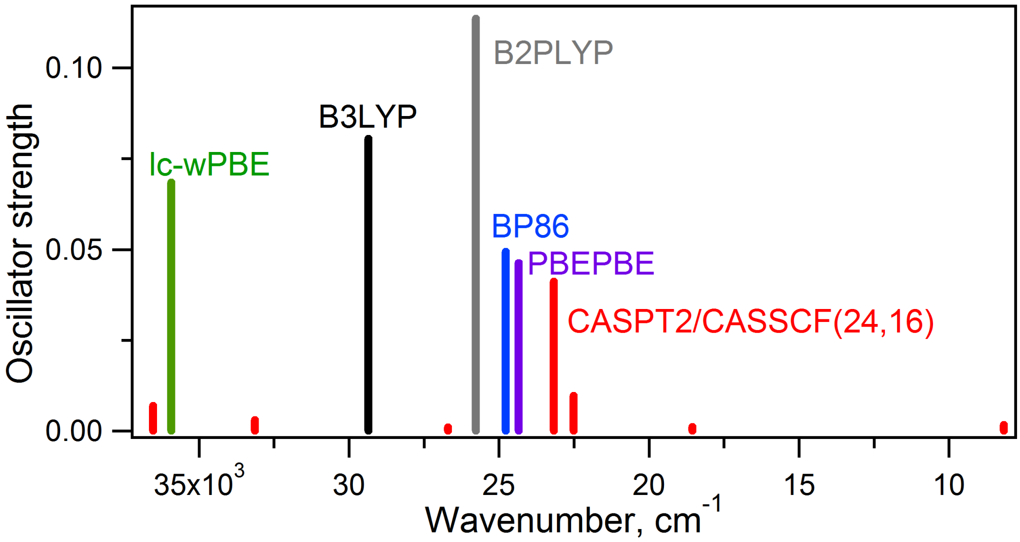

Figure S34. Positions and oscillator strengths of the long-wavelength transition in the electronic absorption spectrum of $[Cu_2I_4]^{2-}$ cluster calculated using TD-DFT/def2-TZVP (with ECP for I) with different functionals. Red bars represent results of SA-CASSCF/CASPT2 calculations.

As dianionic $[Cu_2I_4]^{2-}$ cluster is well separated from the cations, we performed TD-DFT as well as high-level SA-CASSCF/CASPT2[14] calculations of the EAS for isolated cluster. The MOLCAS 7.0 program package[15] was used in the latter case. Figure S34 displays values of the long-wavelength transition predicted at different DFT levels as well as a series of transitions predicted by high-level calculations. Figure S33 demonstrates that LC-ωPBE calculations predict first excitation (cluster-centered, *CC) at about 36000 cm^{-1} (or ~280 nm). However, more accurate SA-CASSF/CASPT2 calculations predict for $[Cu_2I_4]^{2-}$ cluster a series of transitions in the visible region.

Thus, the long-range corrected TD-LC-ωPBE method could correctly reproduce CT-transitions involving molecular MOs localized on the well-separated ligands and Cu_nI_{2n+2} clusters, but it overestimates significantly energies of local excitations. In turn, other employed functionals do not work properly to reproduce CT-transitions. Unfortunately, to use more accurate SA-CASSCF/CASPT2 approach to calculate excited states of compounds **1**–**4** is unrealistic task due to very large systems under study. Nevertheless, we can conclude that despite results of TD-LC-ωPBE calculations, compounds **1**–**4** can have low-lying cluster-centered (*CC) excitations and be involved in the CC-phosphorescence.

§8. References

[1] (*a*) D. A. Bashirov, T. S. Sukhikh, N. V. Kuratieva, E. A. Chulanova, I. V. Yushina, N. P. Gritsan, S. N. Konchenko and A. V. Zibarev, *RSC Adv*., 2014, **4**, 28309–28316; (*b*) T. S. Sukhikh, D. A. Bashirov, D. S. Ogienko, N. V. Kuratieva, P. S. Sherin, M. I. Rakhmanova, E. A. Chulanova, N. P. Gritsan, S. N. Konchenko and A. V. Zibarev, *RSC Adv*., 2016, **6**, 43901–43910.

[2] A. Dreuw and M. Head-Gordon. *Chem. Rev.*, 2005, **105**, 4009–4037.

[3] (*a*) Y. Zhao and D. G. Truhlar, *Acc. Chem. Res*., 2008, **41**, 157–167; (*b*) F. Di Meo, P. Trouillas, C. Adamo and J. C. Sancho-Garcia, *J. Chem. Phys*., 2013, **139**, 164104.

[4] (*a*) A. D. Becke, *Phys. Rev. A*, 1988, **38,** 3098–100; (*b*) J. P. Perdew, *Phys. Rev. B*, 1986, **33**, 8822–8824.

[5] (*a*) A. D. Becke, *J. Chem. Phys.* **1993**, *98*, 5648–5652; (*b*) C. Lee, W. Yang and R. G. Parr, *Phys. Rev. B: Condens. Matter*, 1988, **37**, 785–789.

[6] T. Yanai, D. Tew, N. Handy, *Chem. Phys. Lett*., 2004, **393**, 51–57.

[7] (*a*) O. A. Vydrov and G. E. Scuseria, *J. Chem. Phys*., 2006, *125*, 234109; (*b*) O. A. Vydrov, J. Heyd, A. Krukau and G. E. Scuseria, *J. Chem. Phys*., 2006, *125*, 074106.

[8] Y. Zhao and D. G. Truhlar, *J. Phys. Chem. A*, 2006, **110**, 13126–13130.

[9] S. Grimme, *J. Chem. Phys.*, 2006, **124**, 034108.

[10] (*a*) A. Schäfer, C. Huber and R. Ahlrichs, *J. Chem. Phys*., 1994, **100**, 5829-5835; (*b*) F. Weigend and R. Ahlrichs, *Phys. Chem. Chem. Phys*., 2005, **7**, 3297–3305.

[11] M. J. Frisch, G. W. Trucks, H. B. Schlegel et al., *Gaussian 09, Revision A.01*, Gaussian, Inc., Wallingford CT, 2009.

[12] F. Neese, *Wiley Interdiscip. Rev.: Comput. Mol. Sci.,* **2012**, *2*, 73–78.

[13] (*a*) D. l. M. Zink, M. Bächle, T. Baumann, M. Nieger, M. Kühn, C. Wang, W. Klopper, U. Monkowius, T. Hofbeck, H. Yersin and S. Brase, *Inorg. Chem*., 2013, **52**, 2292⁻2305; (*b*) M. J. Leitl, V. A. Krylova, P. I. Djurovich, M. E. Thompson and H. Yersin, *J. Am. Chem. Soc*., 2014, **136**, 16032−16038; (*c*) G. Li, R. S. Nobuyasu, B. Zhang, Y. Geng, B. Yao, Z. Xie, D. Zhu, G. Shan W. Che, L. Yan, Z. Su, F. B. Dias and M. R. Bryce, *Chem. Eur. J*., 2017, **23**, 11761–11766.

[14] (*a*) K. Andersson and B. O. Roos, in *Modern Electronic Structure Theory*, World Scientific, Singapore, 1995, part 1, vol. 2, pp. 55; (*b*) J. Finley, P.-O. Malmqvist, B. O. Roos and L. Serrano-Andres, *Chem. Phys. Lett*., 1998, **288**, 299–306.

[15] F. Aquilante, L. De Vico, N. Ferre, G. Ghigo, P.-A. Malmqvist, P. Neogrady, T. B. Pedersen, M. Pitonak, M. Reiher, B. O. Roos, L. Serrano-Andres, M. Urban, V. Veryazov and R. Lindh, *J. Comput. Chem*., 2010, **31**, 224–247.